International Journal of Innovation and Industrial Revolution
EISSN: 2637-0972
IJIREV
Volume 6 Issue 17 (June 2024) PP. 232-245
DOI 10.35631/IJIREV.617018


INTERNATIONAL JOURNAL OF INNOVATION AND INDUSTRIAL REVOLUTION (IJIREV)
www.ijirev.com

# EFFECT OF NIOBIUM DOPANT CONCENTRATION ON ZNO NANOSTRUCTURES ON SI POROUS SUBSTRATE

Izzah Nur Zulaikha Masjhur[1,2*], Kevin Alvin Eswar[1,2], Syed Yusainee Syed Yahya[1,2], Mohamad Rusop[1,3], Husairi Fadzilah Suhaimi[1,2]

[1] NANO-SciTech Lab (NST), Centre for Functional Materials and Nanotechnology, Institute of Science, Universiti Teknologi MARA, Shah Alam, Selangor, Malaysia
Email: inzulaikha1303@gmail.com
[2] Faculty of Applied Sciences, Universiti Teknologi MARA (UiTM), 40450 Shah Alam, Selangor, Malaysia
Email: kevinalvin86@uitm.edu.my, syedy237@uitm.edu.my, husairi5840@uitm.edu.my
[3] NANO-ElecTronic Centra (NET), Faculty of Electrical Engineering, Universiti Teknologi MARA (UiTM), 40450 Shah Alam, Selangor, Malaysia
Email: rusop@uitm.edu.my
[*] Corresponding Author

**Article Info:**

**Article history:**
Received date: 28.04.2024
Revised date: 20.05.2024
Accepted date: 15.06.2024
Published date: 30.06.2024

**To cite this document:**

Mashjur, I. N. Z., Eswar, K. A., Yahya, S. Y. S., Rusip, M., & Suhaimi, H. F. (2024). Effect Of Niobium Dopant Concentration On Zno Nanostructures On Si Porous Substrate. *International Journal of Innovation and Industrial Revolution, 6* (17), 232-245.

**DOI:** 10.35631/ IJIREV.617018



**Abstract:**

Zinc oxide (ZnO) nanostructures have gained popularity in sensor technology due to their unique properties and facile device integration. However, the intrinsic optical and electrical properties of ZnO are suboptimal for direct industrial applications, necessitating enhancements through doping. This study investigates the impact of niobium (Nb) doping concentrations on the physical, optical, and electrical characteristics of ZnO nanostructures. FESEM analyses indicate successful deposition of ZnO on silicon nanoparticles substrates, with nanostructure sizes peaking at 88 nm and 115 nm for 6% and 8% Nb dopant concentrations, respectively. XRD results suggest that the structural integrity of the nanostructures is maintained up to a 10% doping level, with an optimal concentration at 6%. UV-Vis spectroscopy shows a shift in the absorption peak into the visible range and a decrease in maximum reflectivity from 47.5990% at 2% doping to 40.9205% at 6% doping, indicating enhanced light absorption suitable for optoelectronic applications. Electrical measurements reveal that a 6% Nb dopant concentration yields the lowest resistivity and highest conductivity among the tested samples. These findings underscore the potential of Nb-doped ZnO nanostructures in improving the performance of optoelectronic devices through tailored doping strategies.

**Keywords:**

Dopant Concentration, Nanostructures, Niobium Dopant, Porous Silicon, Zinc Oxide

International Journal of Innovation and Industrial Revolution
IJIREV
EISSN: 2637-0972
Volume 6 Issue 17 (June 2024) PP. 232-245
DOI 10.35631/IJIREV.617018

## Introduction

Nanotechnology principles are employed extensively across numerous technological advancements and R&D endeavours to improve the effectiveness and dependability of traditional materials. Nanotechnology involves comprehending, directing, and altering matter at incredibly small scales, sometimes as minute as 1000 nanometers, to create novel fundamental characteristics and capabilities. Because of their minute size, nanomaterials frequently exhibit distinct physical or chemical attributes compared to their larger counterparts. Nanoparticles have demonstrated extensive usefulness because of their distinct physiochemical properties counting the changes in magnetic biochemical, electronic and optical properties at atomic, cellular as well as molecular levels due to their high surface-to-volume ratio (Yin & Zhong, 2020). Discoveries in the past decade have proven that once materials are arranged in the shape of very small atoms, they significantly change their physical and chemical properties, even to the extent that completely new phenomena are formed (Sharma, Jandaik, Singh, & Kumar, 2016).

One favourable nanostructure that is most used and researched on is ZnO. The definite properties of ZnO such as a large band gap of 3.3eV, high exciton binding energy of 60meV, good chemical and thermal stability, as well as high mobility of conducting electrons, makes it an outstanding contestant for varying electronic devices applications like gas sensors, solar cells, LEDs, lasers, photo detectors, and nano-generators (Rajan, Periasamy, & Sahula, 2016). It is also one of the most favourable materials for the fabrication of the next generation of optoelectronics devices in the UV region and optical or display devices (Wisz, Virt, Sagan, Potera, & Yavorskyi, 2017).

In semiconductor industries, characteristic, availability and cost are the main consideration in device fabrication. In ZnO synthesisation, most researchers have chosen silicon-based substrate due to its abundance in the Earth"s crust. This advantage leads to low-cost in bulk production. In addition, its characteristics, such as high resistivity, was also considered. Consequently, Silicon-ZnO thin films appear to be a very important transparent conducting oxide material for Si-based electronic devices (M. Das, Sarmah, Barman, Sarma, & Sarkar, 2020). Even though advantageous in term of cost fabrication, some problems have been found when the silicon was used as a substrate in ZnO nanostructure deposition. The layer of nanostructured ZnO film was easy to peel off from the silicon surface. This may be good for ZnO powder synthesisation, but it is not suitable for optoelectronic devices applications. This is because it needs a strong attachment between the material and substrate. The significant disparity in lattice structures between ZnO and the silicon surface was thought to be the cause of this occurrence (L.-l. Chen, Zhai, & Huang, 2020). Therefore, some modifications are required on the silicon surface to overcome this problem.

Over the last decades, in efforts to increase the capabilities of silicon technology, porous silicon has been the focus of attention to achieve it. Silicon porosification is a convenient and uncomplicated method of nanostructuring and its properties are remarkedly different than the properties of bulk materials (Korotcenkov, 2016; Vercauteren, Scheen, Raskin, & Francis, 2021). Consequently, interest in porous silicon rose significantly as it was established that the nanostructured and biodegradable material possesses a range of properties and it was applied in many fields such as micro and optoelectronics, photonics, medical science, chemical sensing and bioengineering.

International Journal of Innovation and Industrial Revolution
EISSN: 2637-0972 IJIREV
Volume 6 Issue 17 (June 2024) PP. 232-245
DOI 10.35631/IJIREV.617018

Scientist have dedicated their effort for the preparation of novel doped nanostructures since its discovery as well as boundless research has been concentrated on the different applications of the doped nanostructures (Liu & Engineering, 2019). Numerous academics have investigated how dopants affect ZnO thin films. Some studied and more commonly used dopant of ZnO are Al, Ga, In and F which produce single charge carrier per dopant atom (D. Das & Karmakar, 2020), however a study on Niobium, Nb doping onto ZnO is still insufficient but what has been found by Kruefu, Liewhiran, Wisitsoraat, and Phanichphant (2011) is promising. He investigated the potential of Nb-doped ZnO in gas sensor applications especially as Nb5+ and Zn2+ share three valence elections, where the electrical conductivity can be increased by three valence electrons per Nb atom.

The distinctive and captivating properties of doped nanostructures materials have set off immense motivation among researchers to explore the prospect of using it in technological applications (Wisz et al., 2017). Mainly doped nanostructures' electronic and optical properties are under scrutiny due to its promising implementation in the fabrication of micro and optoelectronic devices. ZnO nanostructures have gained popularity in recent years due to their ease of production and unique properties. However, due to its poor optical and electrical properties, intrinsic ZnO cannot be used directly (Bharat et al., 2019). As a result, they are not suited for direct use in the industry. To address these concerns, dopants were added to the nanostructured ZnO to increase its characteristics. The incorporation of metallic dopants is recognized to alter various physical properties of pristine semiconductor materials (Mohammedi, Ibrir, Meglali, & Berri, 2021). Doping ZnO with noble metal materials is a finer method for the improvement of an electronic device as it has a greater conductivity, acceptable carrier charge, easier to achieve and control, higher transpiracy and better stability (R.-q. Chen, Zou, Yan, & Gao, 2011).

## Methodology

The research will be done in three main activities. First the porous silicon will be synthesized using anodization method. Then will be the nanostructured ZnO films deposited on SiNPs as a seed layer by spin coating method. In this method, zinc acetate dihydrate and diethanolamine (DEA) and isopropyl were used as a starting material, stabilizer and solvent respectively.

Next will be the synthesis of ZnO doped with niobium using immersion method with different dopant concentration. The immersion method uses zinc nitrate hexahydrate as a precursor, HMTA as a stabilizer and niobium chlorate (NbCl5) as a dopant.

The characterization of materials such as morphology, optical and electrical properties. Surface morphologies of ZnO nanostructures were studied using FESEM and its structural properties using XRD spectrometer. Furthermore, its optical property is analysed using UV-Vis spectroscopy and the electrical property is investigated using I-V 2-probe and Hall effect measurement.

## Result And Discussion

### *Structural Properties*

The samples were subjected to concentration-dependent experiments to understand the properties of ZnO grown with different molecular weight percentage of Nb dopant. The morphological evolution of Nb-doped ZnO on SiNPs substrate were examined using FESEM

International Journal of Innovation and Industrial Revolution
IJIREV
EISSN: 2637-0972
Volume 6 Issue 17 (June 2024) PP. 232-245
DOI 10.35631/IJIREV.617018

images. Figure 1 shows FESEM images for (a) SiNPs, (b) 2%, (c) 4%, (d) 6%, (e) 8% and (f) 10% molecular weight percentage of Nb-dopant. at 10k magnification. As seen in Fig 1(a), the irregular pores with sizes in the range of ~10 to ~22 nm were observed over the SiNPs surface. Besides, it can be seen that the distribution of the pores is irregular. The pores indicate that the surface area of the silicon has increased.

FESEM images provided further insight, demonstrating the successful growth of ZnO nanoparticles on the seeded SiNPs thin film. The abundance and uniform distribution of the ZnO nanoparticles resulted in the porosity of the seeded SiNPs thin film being indiscernible. The samples were effectively covered, eliminating the need for coating with conductive metals such as gold or platinum before FESEM analysis, as the light was well-reflecting. Previous studies suggest that the SiNPs layer serves as a favorable substrate for reducing lattice mismatch heteroepitaxy. This is attributed to ZnO nanoparticles infiltrating into the pores and establishing conducive nucleation sites, promoting preferred orientation during growth (Barala, Maidur, Mohan, & Sanghi, 2022).

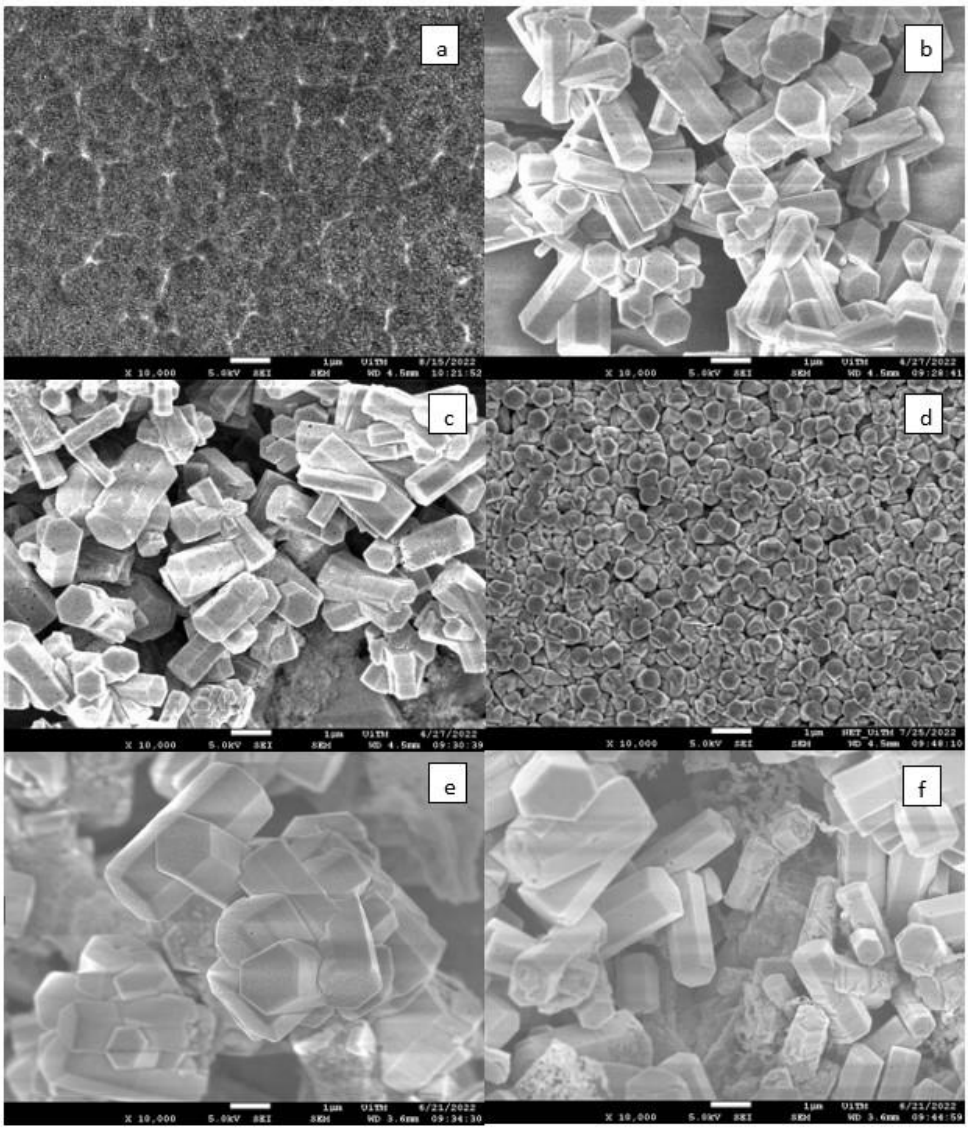


**Figure 1: FESEM images of a) SiNPs, and ZnO Nanostructures Doped With Different Molecular Weight of Nb; b) 2%, c) 4%, d) 6%, e) 8% and f) 10%**

International Journal of Innovation and Industrial Revolution
EISSN: 2637-0972
IJIREV
Volume 6 Issue 17 (June 2024) PP. 232-245
DOI 10.35631/IJIREV.617018

All the particles were made up of hexagonal wurtzite as is expected from ZnO however the sizes of each particle varied with different concentration of molecular weight of Nb dopant. The changes in the size of particles show the effect of the Nb dopant in influencing the size of the nanostructures. The variation in diameter size results from the differences in the ionic radii between dopant and Zn which influences the attractive forces between the atoms and hence reduces the diameter size of the ZnO nanostructures.

Figure 2, an energy-dispersive X-ray spectroscopy (EDS) analysis of the 6% Nb-doped ZnO nanostructure which shows that Nb was successfully incorporated into the ZnO. The EDS analysis shows presence of Zn, Nb and Si as expected, no other impurity elements were present in the structure.

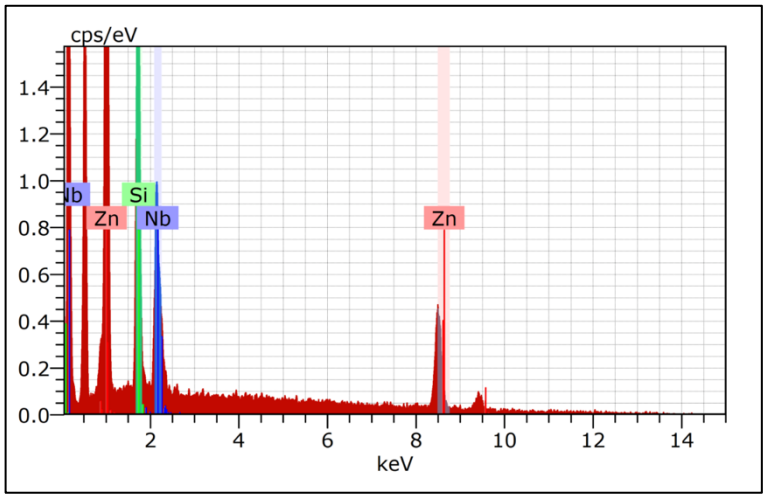


**Figure 2: EDS Spectra of Nb-doped ZnO Nanostructure**

Typical XRD patterns of ZnO nanostructures with different concentrations of Nb dopant were analyzed to explore the influence of morphology on the properties of the nanostructure as shown in Figure 3. Several diffraction peaks appeared in the spectra of the doped ZnO nanostructures from 20° to 50°, corresponding to the (100), (002), (101) and (102) directions of the hexagonal ZnO wurtzite with lattice parameters a, b = 3.25Å and c = 5.21Å as according to JCPDS no. 16-1451 (Djurišić, Ng, & Chen, 2010). However, there is a peak between the peak (100) and (002) that corresponds to the Si substrate at approximately 33.2° for all samples.

International Journal of Innovation and Industrial Revolution
EISSN: 2637-0972
Volume 6 Issue 17 (June 2024) PP. 232-245
DOI 10.35631/IJIREV.617018

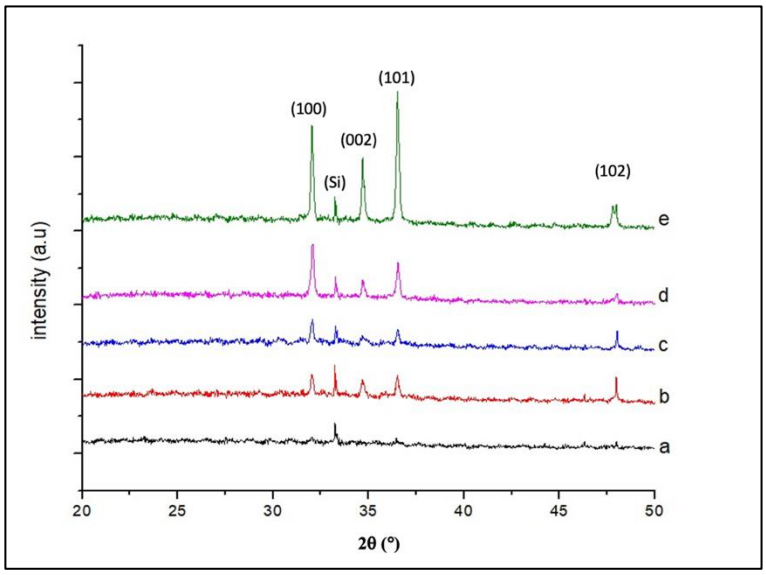


**Figure 3: XRD Spectra of a) 2%, b) 4%, c) 6%, d) 8% and e) 10% Molecular Weight of Nb Dopant**

The intensity of the (002) peak is sharper with increasing concentration of the dopant, indicating that the preferred growth orientation of the grown ZnO microrods is moving towards the *c*-axis which can be related to the low surface free energies of the (002) plane (Luo et al., 2020). The strong intensity and narrow width of the ZnO diffraction peaks indicates that the ZnO nanostructure have good crystallinity. The observed shift in the 2θ angle towards higher values as the Nb content increases may be attributed to differences in the radii of the Zn and Nb ions, respectively (Li et al., 2020). Specifically, the substitution of Zn ions by Nb-dopant ions causes the peak 2θ angle to shift to a higher value due to the smaller ionic radius of Nb (0.67Å) compared to that of Zn (0.74Å).

Table 1 shows the value of the plane distance, peak position, crystallite size and FWHM of the effect of dopant on the ZnO nanostructures. The estimation of crystallite size, D, based on plane distance for each plane was calculated using Bragg's equation, as shown in Equation 1 and the crystallite size can be calculated using Scherrer's equation as shown in Equation 2.

$$\lambda = 2d \sin \theta \quad (4.1)$$

$$D = \frac{0.89\lambda}{\beta cos\theta} \quad (4.2)$$

The peak position of plane (100) slightly shifted to a higher diffraction angle when the concentration of dopant is increased but it remained constant from 6% doped onwards. The same can be said for peak position (002) where from 2% to 4%, it shifted to a higher diffraction angle but then shifted lower at 6% where it remained for the rest of the dopant concentration. It has been suggested that the diffraction angle shifts due to the effect of stress or imperfection of the crystalline of ZnO nanostructures (Gao et al., 2012; Marin-Ramirez, Gonzalez Lemus, Budini, Tirado, & Comedi, 2020). Crystallite size showed that ZnO nanostructures was biggest at 6% of Nb doping concentration compared to the rest with 54.24 nm respectively. The size remained unchanged with higher doping concentration.

The absence of a diffraction peak related to Nb in the doped samples is attributed to the small amount of added Nb falling below the detection limit. This observation indicates that no

International Journal of Innovation and Industrial Revolution
EISSN: 2637-0972 IJIREV
Volume 6 Issue 17 (June 2024) PP. 232-245
DOI 10.35631/IJIREV.617018

compounds involving Nb have been formed in the samples (Zeng, Liu, & Wang, 2012). It reveals that the metal ions occupy interstitial position and do not change the hexagonal wurtzite structure. Nevertheless, the sharpness of the peak with increases concentration of Nb-dopant shows the successful presence of Nb in ZnO thin film. Where the presence of Nb in ZnO thin films reduces the disorder and carrier scattering because of the replacement of $Nb^{5+}$ with $Zn^{2+}$ (Hammad, Abdel-wahab, & jilani, 2020). This result had been supported by Figure 2, The EDS analysis of the Nb-doped ZnO nanostructure which shows that even though it was unable to be detected in the XRD spectra, the Nb was successfully incorporated into the ZnO.

**Table 1: The XRD Data for The Effect of Dopant on ZnO Nanostructures.**

| Dopant Concentration | Lattice Orientation | Peak position, 2θ (°) | FWHM (°) | d-spacing (nm) | Crystallite size, D (nm) |
|---|---|---|---|---|---|
| 2% | 100 | 31.69 | 0.29 | 0.2820 | 29.72 |
| | 002 | 34.38 | 0.20 | 0.2606 | 43.39 |
| | 101 | 38.18 | 0.27 | 0.2481 | 32.49 |
| 4% | 100 | 31.84 | 0.22 | 0.2808 | 39.19 |
| | 002 | 34.50 | 0.18 | 0.2597 | 48.23 |
| | 101 | 36.34 | 0.24 | 0.2470 | 36.36 |
| 6% | 100 | 32.07 | 0.22 | 0.2789 | 39.21 |
| | 002 | 34.47 | 0.16 | 0.2600 | 54.25 |
| | 101 | 36.53 | 0.18 | 0.2458 | 48.50 |
| 8% | 100 | 32.07 | 0.19 | 0.2789 | 45.40 |
| | 002 | 34.47 | 0.16 | 0.2600 | 54.25 |
| | 101 | 36.53 | 0.18 | 0.2458 | 48.50 |
| 10% | 100 | 32.07 | 0.19 | 0.2789 | 45.40 |
| | 002 | 34.47 | 0.16 | 0.2600 | 54.25 |
| | 101 | 36.53 | 0.18 | 0.2458 | 48.50 |

***Optical Properties***

Figure 4 shows the result of UV-vis reflectance between different molecular weight of Nb doping concentration onto ZnO nanostructure with immersion time kept at 4 hours and the immersion temperature at 90°C. The sample is illuminated by spectra in the wavelength region of 300 nm to 800 nm. At 350 nm for all the samples, there's a rise in peak where it shifted over to the visible range with a significant decrease of the maximum reflectivity from 47.5990 % (2% Nb dopant concentration) to 40.9205 % (6% Nb dopant concentration) which suggest that the higher dopant concentration has low reflectance and high absorbance which makes it an ideal candidate for optoelectronic devices. This reveals that the attenuation of the reflectivity with increasing concentration of dopant is due to trapping effect (Youssef, El-Nahass, El-Zaiat, & Altalbawy, 2018).

The figure 5 further show the extrapolation of a straight line using Tauc's plot where α is calculated using Kubelka-Munk relation $[h\nu \ln [(R_{max} - R_{min}) / (R - R_{min})]^{1/2}$ vs $E_g$. The result of the diffuse reflectance measurements used for determination of the absorption coefficient using [K-M or F(R)] relation for Tauc's Equation was stated in equation (2.3) and (2.4). The results are tabulated in Table 4.3 and it states the value of the energy gap for the samples (a) to (e) as well as the $R_{maximum}$ and $R_{minimum}$ obtained.

International Journal of Innovation and Industrial Revolution
EISSN: 2637-0972
IJIREV
Volume 6 Issue 17 (June 2024) PP. 232-245
DOI 10.35631/IJIREV.617018

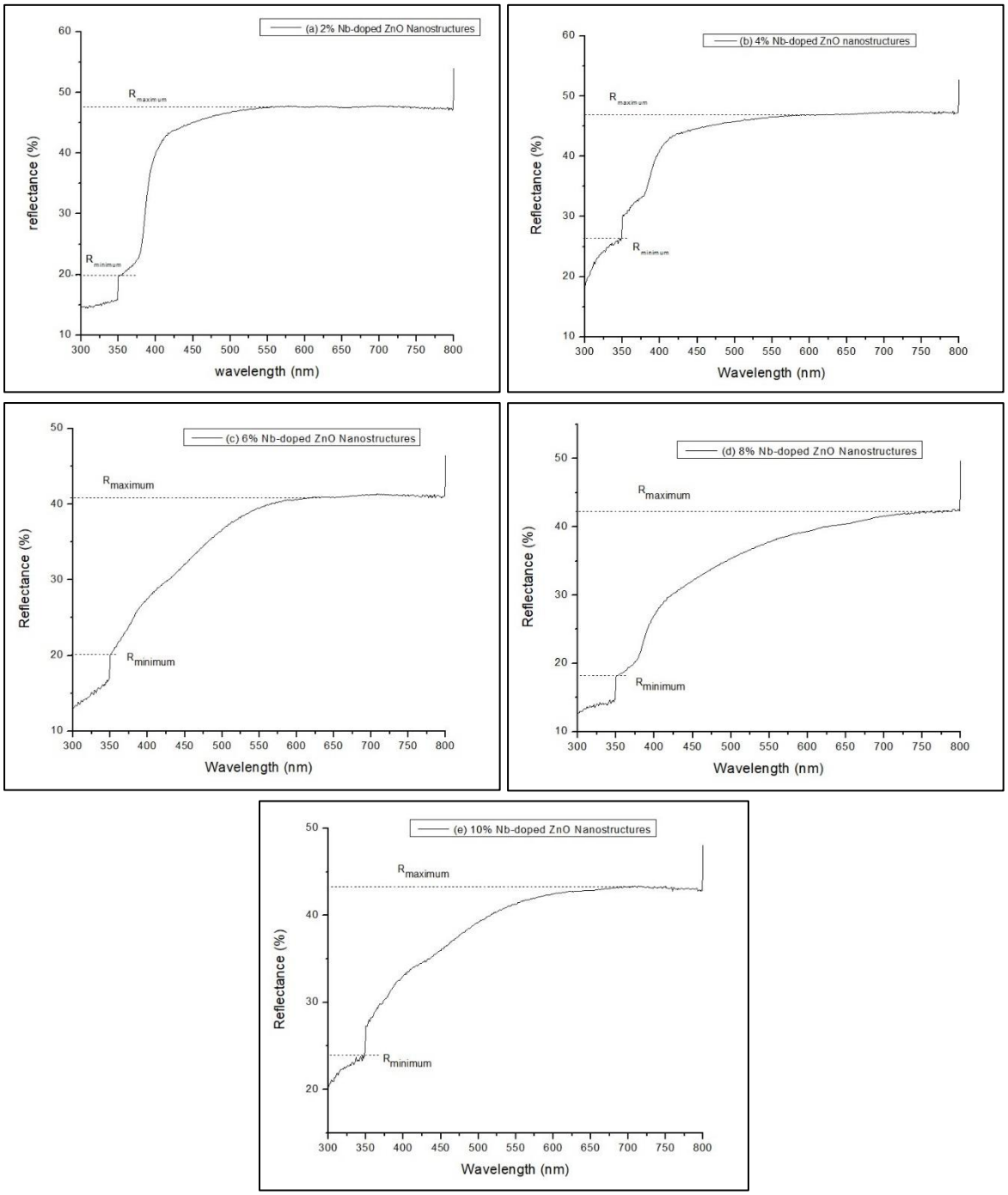


**Figure 4: UV-Vis Reflectance Between Different Molecular Weight of Nb Doping Concentration onto ZnO Nanostructure**

International Journal of Innovation and Industrial Revolution
EISSN: 2637-0972
Volume 6 Issue 17 (June 2024) PP. 232-245
DOI 10.35631/IJIREV.617018

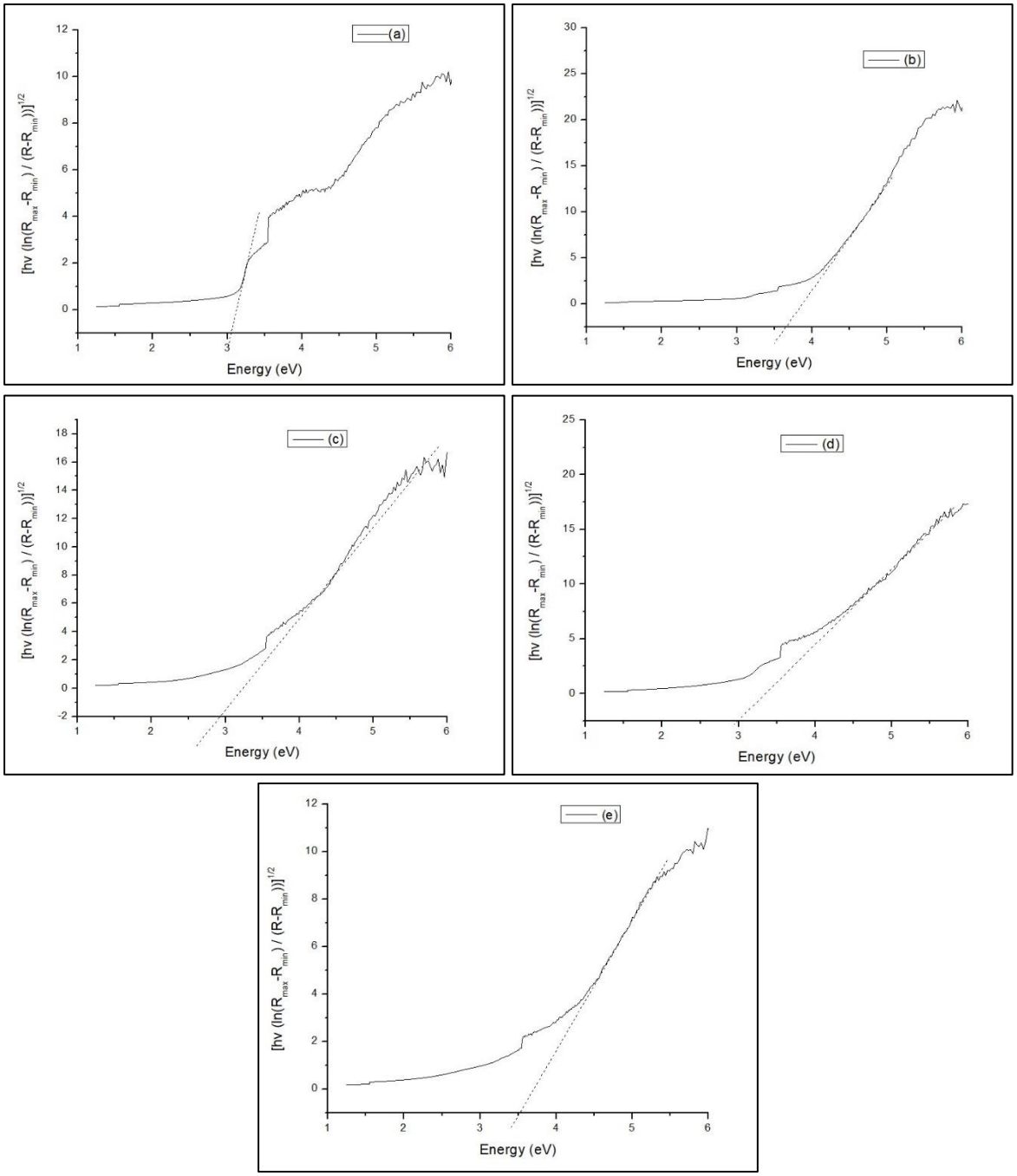


**Figure 5: The Extrapolation of a Straight Line using Tauc's Plot, where α is Calculated using Kubelka-Munk Relation [*hν* ln [($R_{max}$ – $R_{min}$) / (R – $R_{min}$)]$^{1/2}$ vs $E_g$ between Different Molecular Weight of Nb Doping Concentration onto ZnO Nanostructure**

Based from the tabulated data in Table 2, 6% Nb doped ZnO nanostructures had the lowest energy gap which is at 2.9351 eV. However, increasing more of the dopant concentration to 8% and 10%, the energy gap increases with the highest being at 3.5272 eV. The doping of Nb onto ZnO shows favorable result as it decreases the energy gap from ZnO standard of 3.37 eV as lower energy gap gives devices the ability to operate at low temperatures (Jang et al., 2019).

International Journal of Innovation and Industrial Revolution
EISSN: 2637-0972 IJIREV
Volume 6 Issue 17 (June 2024) PP. 232-245
DOI 10.35631/IJIREV.617018

**Table 2: Data of Energy Gap of Samples with Different Molecular Weight Percentage of Nb Dopant.**

| Sample | Nb dopant (wt%) | $R_{max}$ (%) | $R_{min}$ (%) | Energy gap using Kubelka-Munk $Eg = [h\nu \ln [(R_{max} - R_{min}) / (R - R_{min})]^{1/2}$ (eV) |
|---|---|---|---|---|
| (a) | 2 | 47.5990 | 19.7378 | 3.0489 |
| (b) | 4 | 46.8752 | 25.4026 | 3.6628 |
| (c) | 6 | 40.9205 | 20.1284 | 2.9351 |
| (d) | 8 | 42.2518 | 18.2109 | 2.9940 |
| (e) | 10 | 43.2887 | 23.9293 | 3.5272 |

***Electrical Properties***

The study of electrical properties of the material is really necessary since the presence of dopants plan an important role to the conductivity of the thin films. In this research, the electrical characteristics of the prepared materials were examined by using a two-point probe *I-V* measurement system at room temperature under UV-illumination, and the result is shown in Figure 6. The metal contact (gold) was deposited onto the thin films as an electrode to obtain the measurement of *I-V* characteristics. The result is shown in Figure 4.6 where (a) to (e) is the Nb-dopant concentration from 2% to 10%.

All samples showed a linear response, which indicates good ohmic contact with the sample (Mohamed Zahidi et al., 2022). Based on the I-V curve, the samples exhibit ohmic behavior that obeys Ohm's law which states that the current is directly proportional to the voltage or potential difference through a conductor between two points. Figure 4.6 shows that when the applied voltage was increased from -5 to 5 V, the results showed a decrease in current density as more Nb dopant concentration was introduced.

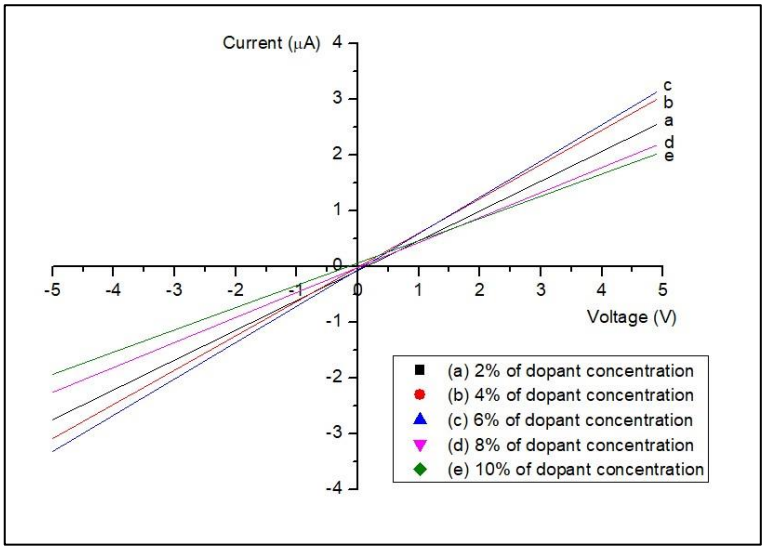


**Figure 6: The *I-V* Curve of Different Molecular Weight Percentage of Nb Dopant on ZnO Nanostructures**

International Journal of Innovation and Industrial Revolution
IJIREV
EISSN: 2637-0972
Volume 6 Issue 17 (June 2024) PP. 232-245
DOI 10.35631/IJIREV.617018

The resistivity, ρ and the conductivity σ were investigated by using equation (2.5) and (2.6) with the values stated and the calculated resistivity and conductivity value of the thin films are listed in Table 3. From Table 3, it is noticed that the electrical measurement reveals the addition of Nb dopant increases the resistance of the sample. The increase in resistivity can be attributed to the shallow acceptor nature of the impurities (Al-Ariki et al., 2021; Singh & Rao, 2009). In such cases, the electrons from donor levels, specifically the Zn interstitials and oxygen vacancies, are available but get trapped by the divalent ions. This trapping phenomenon leads to a decrease in the concentration of n-type donor carriers, subsequently causing an increase in resistivity.

**Table 3: Resistance, Resistivity, and Conductivity Value of Different Molecular Weight Percentage of Nb Dopant on ZnO Nanostructures**

| | Dopant Concentration | Resistance (μΩ) | Resistivity, ρ (Ω nm) | Conductivity, σ (S $nm^{-1}$) |
|---|---|---|---|---|
| (a) | 2% | 1.8727 | 0.515 | 1.942 |
| (b) | 4% | 1.6298 | 0.448 | 2.231 |
| (c) | 6% | 1.5377 | 0.423 | 2.365 |
| (d) | 8% | 2.2352 | 0.615 | 1.627 |
| (e) | 10% | 2.5076 | 0.690 | 1.450 |

Based on the tabulated data in Table 3, 6% dopant concentration had the lowest resistivity at 0.423 Ω nm and the highest conductivity at 2.365 S $nm^{-1}$. This result is consistent with previous result where 6% of Nb dopant concentration had the lowest energy gap according to the Kubelka-Munk relation in Chapter 4.2.2. The low resistivity and high conductivity makes it suitable for optoelectronic devices (Wang & Qi, 2019).

The Hall effect measurement was carried out using a four-point probe, and the result is tabulated in Table 4. The carrier concentration of Nb-doped ZnO showed a rise from 1.401 x $10^{14}$ $cm^{-3}$ at 2% molecular weight concentration to 1.913 x $10^{14}$ $cm^{-3}$ at 6% molecular weight concentration where it further then decreases at 8% and 10%. An increment in donor carrier concentration brings the Fermi level up in the energy gap and results in the reduction of activation energy (Vipul & Amit, 2020).

**Table 4: Carrier Concentration and Carrier Mobility of Different Nb-doped Concentration on ZnO Thin Films.**

| | Dopant Concentration | Carrier Concentration (x$10^{14}$ $cm^{-3}$) | Carrier Mobility (x$10^{3}$ $cm^2/(V.s)$) |
|---|---|---|---|
| (a) | 2% | 1.401 | 3.480 |
| (b) | 4% | 1.636 | 3.335 |
| (c) | 6% | 1.913 | 2.949 |
| (d) | 8% | 1.573 | 2.023 |
| (e) | 10% | 1.521 | 1.647 |

## Conclusion

In conclusion, for the effect of dopant concentration on ZnO nanostructures, it has been investigated in terms of surface and morphology, optical and electrical properties. FESEM

International Journal of Innovation and Industrial Revolution
EISSN: 2637-0972 IJIREV
Volume 6 Issue 17 (June 2024) PP. 232-245
DOI 10.35631/IJIREV.617018

results showed that the ZnO was successfully deposited onto the SiNPs substrate with the largest nanostructure at 6% and 8% molecular weight of dopant concentration which is 88 and 115 nm respectively. The XRD data showed that the the nanostructures peaked at 6% and remained constant even for 8% and 10% dopant concentration. This allowed expectations that 6% is the optimum dopant concentration for Nb-doped ZnO nanostructures.

The UV-Vis result revealed that at 350 nm for all the samples, there's a rise in peak where it shifted over to the visible range with a significant decrease of the maximum reflectivity from 47.5990 % (2% Nb dopant concentration) to 40.9205 % (6% Nb dopant concentration) which suggest that the higher dopant concentration has low reflectance and high absorbance which makes it an ideal candidate for optoelectronic devices. This is also further supported by the electrical result where the I-V measurement showed that the 6% of dopant concentration had the lowest resistivity and the highest conductivity among all the samples.

Conclusively, the doping of Nb in ZnO nanostructures significantly enhances their optical and electrical properties, positioning them as promising candidates for future optoelectronic devices. Future studies could explore further optimizations of dopant concentrations beyond 6% to understand their full potential in practical applications, such as solar cells and sensors, thereby advancing the field of nanostructured metal oxide materials.

## Acknowledgments

The authors wish to acknowledge the Faculty of Applied Sciences at Universiti Teknologi MARA, Shah Alam, Selangor, Malaysia for providing the facilities and financial support for this research.

## References

Al-Ariki, S., Yahya, N. A. A., Al-A'nsi, S. a. A., Jumali, M. H. H., Jannah, A. N., & Abd-Shukor, R. (2021). Synthesis and comparative study on the structural and optical properties of ZnO doped with Ni and Ag nanopowders fabricated by sol gel technique. *Scientific Reports, 11*(1), 11948. doi:10.1038/s41598-021-91439-1

Barala, M., Maidur, S. R., Mohan, D., & Sanghi, S. (2022). Third order nonlinearity and optical power limiting studies of PS/ZnO nanocomposite foils for photonic applications. *Physica Scripta, 97*(10), 105501. doi:10.1088/1402-4896/ac8b42

Bharat, T. C., Shubham, Mondal, S., S.Gupta, H., Singh, P. K., & Das, A. K. (2019). Synthesis of Doped Zinc Oxide Nanoparticles: A Review. *Materials Today: Proceedings, 11*, 767-775. doi:https://doi.org/10.1016/j.matpr.2019.03.041

Chen, L.-l., Zhai, B.-g., & Huang, Y. M. (2020). Rendering Visible-Light Photocatalytic Activity to Undoped ZnO via Intrinsic Defects Engineering. *Catalysts, 10*(10). doi:10.3390/catal10101163

Chen, R.-q., Zou, C.-w., Yan, X.-d., & Gao, W. (2011). Zinc oxide nanostructures and porous films produced by oxidation of zinc precursors in wet-oxygen atmosphere. *Progress in Natural Science: Materials International, 21*(2), 81-96. doi:https://doi.org/10.1016/S1002-0071(12)60041-0

Das, D., & Karmakar, L. (2020). Optimization of Si doping in ZnO thin films and fabrication of n-ZnO:Si/p-Si heterojunction solar cells. *Journal of Alloys and Compounds, 824*, 153902. doi:https://doi.org/10.1016/j.jallcom.2020.153902

Das, M., Sarmah, S., Barman, D., Sarma, B. K., & Sarkar, D. (2020). Distinct band UV–Visible photo sensing property of ZnO-Porous silicon (PS):p-Si hybrid MSM heterostructure.

International Journal of Innovation and Industrial Revolution
IJIREV
EISSN: 2637-0972
Volume 6 Issue 17 (June 2024) PP. 232-245
DOI 10.35631/IJIREV.617018

*Materials Science in Semiconductor Processing, 118*, 105188. doi:https://doi.org/10.1016/j.mssp.2020.105188

Djurišić, A. B., Ng, A. M. C., & Chen, X. Y. (2010). ZnO nanostructures for optoelectronics: Material properties and device applications. *Progress in Quantum Electronics, 34*(4), 191-259. doi:https://doi.org/10.1016/j.pquantelec.2010.04.001

Gao, K., Li, Q., Hu, Z., Yu, W., Sun, J., Xu, N., & Wu, J. (2012). Correlation between structure and photoluminescence of c-axis oriented nanocrystalline ZnO films and evolution of photo-generated excitons. *Solar Energy Materials and Solar Cells, 96*, 117-123. doi:https://doi.org/10.1016/j.solmat.2011.09.033

Hammad, A. H., Abdel-wahab, M. S., & jilani, A. (2020). Characterization of niobium-doped zinc oxide thin films: Structural changes and optical properties. *Materials Today Communications*, 101791. doi:https://doi.org/10.1016/j.mtcomm.2020.101791

Jang, J. S., Kim, J., Ghorpade, U., Shin, H. H., Gang, M. G., Park, S. D., . . . Kim, J. H. (2019). Comparison study of ZnO-based quaternary TCO materials for photovoltaic application. *Journal of Alloys and Compounds, 793*, 499-504. doi:https://doi.org/10.1016/j.jallcom.2019.04.042

Korotcenkov, G. (2016). *Porous Silicon: From Formation to Application: Formation and Properties,* Volume One: CRC Press.

Kruefu, V., Liewhiran, C., Wisitsoraat, A., & Phanichphant, S. (2011). Selectivity of flame-spray-made Nb/ZnO thick films towards NO2 gas. *Sensors and Actuators B: Chemical,* 156(1), 360-367. doi:https://doi.org/10.1016/j.snb.2011.04.046

Li, C.-Y., Lin, C.-C., Chu, S.-Y., Lin, J.-T., Huang, C.-Y., & Hong, C.-S. (2020). Effects of Nb doping on switching-voltage stability of zinc oxide thin films. *Journal of Applied Physics, 128*(17), 175308. doi:10.1063/1.5140027

Luo, S., Liu, C., Zhou, S., Li, W., Ma, C., Liu, S., . . . He, S. (2020). ZnO nanorod arrays assembled on activated carbon fibers for photocatalytic degradation: Characteristics and synergistic effects. *Chemosphere, 261*, 127731. doi:https://doi.org/10.1016/j.chemosphere.2020.127731

Marin-Ramirez, O., Gonzalez Lemus, N., Budini, N., Tirado, M., & Comedi, D. (2020). The influence of methanol and NH4Cl on solvothermal ZnO synthesis and properties. *Applied Physics A, 126*, 466. doi:10.1007/s00339-020-03636-w

Mohamed Zahidi, M., Mamat, M. H., Malek, M. F., Yaakob, M. K., Ahmad, M. K., Abu Bakar, S., . . . Mahmood, M. R. (2022). Evaluating Different TiO2 Nanoflower-Based Composites for Humidity Detection. *Sensors, 22*(15), 5794.

Mohammedi, A., Ibrir, M., Meglali, O., & Berri, S. (2021). Influence of Cu-Doping on Linear and Nonlinear Optical Properties of High-Quality ZnO Thin Films Obtained by Spin-Coating Technique. *physica status solidi (b), 258*(5), 2000472. doi:https://doi.org/10.1002/pssb.202000472

Rajan, L., Periasamy, C., & Sahula, V. (2016). Electrical characterization of Au/ZnO thin film Schottky diode on silicon substrate. *Perspectives in Science, 8*, 66-68. doi:https://doi.org/10.1016/j.pisc.2016.03.011

Sharma, N., Jandaik, S., Singh, T. G., & Kumar, S. (2016). Chapter 14 - Nanoparticles: Boon to mankind and bane to pathogens. In A. M. Grumezescu (Ed.), *Nanobiomaterials in Antimicrobial Therapy* (pp. 483-509): William Andrew Publishing.

Singh, S., & Rao, M. S. R. (2009). Optical and electrical resistivity studies of isovalent and aliovalent $3d$ transition metal ion doped ZnO. *Physical Review B, 80*(4), 045210. doi:10.1103/PhysRevB.80.045210

International Journal of Innovation and Industrial Revolution
EISSN: 2637-0972 IJIREV
Volume 6 Issue 17 (June 2024) PP. 232-245
DOI 10.35631/IJIREV.617018

Vercauteren, R., Scheen, G., Raskin, J.-P., & Francis, L. A. (2021). Porous silicon membranes and their applications: Recent advances. *Sensors and Actuators A: Physical, 318*, 112486. doi:https://doi.org/10.1016/j.sna.2020.112486

Vipul, S., & Amit, P. D. (2020). Effect of doping concentration on optical and electrical properties of intrinsic n-type ZnO (i-ZnO) and (Cu, Na and K) doped p-type ZnO thin films grown by chemical bath deposition method. *Наносистемы: физика, химия, математика, 11*(4), 391-400.

Wang, W., & Qi, L. (2019). Light Management with Patterned Micro- and Nanostructure Arrays for Photocatalysis, Photovoltaics, and Optoelectronic and Optical Devices. *Advanced Functional Materials, 29*(25), 1807275. doi:https://doi.org/10.1002/adfm.201807275

Wisz, G., Virt, I., Sagan, P., Potera, P., & Yavorskyi, R. (2017). Structural, Optical and Electrical Properties of Zinc Oxide Layers Produced by Pulsed Laser Deposition Method. *Nanoscale Research Letters, 12*(1), 253. doi:10.1186/s11671-017-2033-9

Yin, L., & Zhong, Z. (2020). 1.3.8B - Nanoparticles. In W. R. Wagner, S. E. Sakiyama-Elbert, G. Zhang, & M. J. Yaszemski (Eds.), *Biomaterials Science (Fourth Edition)* (pp. 453-483): Academic Press.

Youssef, G. M., El-Nahass, M. M., El-Zaiat, S. Y., & Farag, M. A. (2016). Investigation of size and band gap distributions of Si nanoparticles from morphology and optical properties of porous silicon layers formed on a textured N+ P silicon solar cell. *Int. J. Semicond. Sci. Technol*, *6*, 1-12.

Zeng, W., Liu, T., & Wang, Z. (2012). Impact of Nb doping on gas-sensing performance of TiO2 thick-film sensors. *Sensors and Actuators B: Chemical*, *166*, 141-149.